ADVANCED ENGINEERING MATERIALS

DOI: 10.1002/adem.201600116

Influence of Structural Defects on the Electrical Properties of Carbon Nanotubes and Their Polymer Composites**

By *G. Domínguez-Rodríguez, A. Tapia, G. D. Seidel* and *F. Avilés**

The influence of carbon nanotube (CNT) structural damage (CNTSD) on the axial and transverse electrical conductivities of CNT/polymer composites is explored through a hierarchical multiscale modeling strategy. The composite cylinder and Mori–Tanaka's methods are used to model effective representative volume elements of CNT/polymer composites containing different fractions of defects. The axial and transverse CNT conductivities are adversely influenced by CNTSD, with the decrease being more pronounced for small radius CNTs. The predictions indicate that an 8% fraction of CNTSD decreases the axial and transverse conductivities of composites containing randomly oriented CNTs by 25–30%. Similar reductions in conductivity are found for both random and clustered damage.

1. Introduction

The applications of polymer composites reinforced by the addition of carbon nanotubes (CNTs) are numerous, specially for situations where low density, high strength, and multifunctionality are relevant.[1] The mechanical, and especially electrical properties of polymers are drastically enhanced by the addition of low volume fractions of CNTs, creating multifunctional materials.[2–4] A theoretical formulation based on chirality exists to predict the CNT electrical behavior,[5] and it is accepted that armchair singlewall CNTs (SWCNTs) are metallic,[6,7] that is, without a bandgap. Therefore, CNTs render polymer composites with sufficient electrical conductivity to produce multifunctional materials which may be used, for example, as strain sensors.[8,9]

Different forms of structural damage have been reported for CNTs and other graphene-like structures. One of the most common and severe form of damage are vacancies, that is, missing atoms in the periodic structure.[10,11] Vacancies can be single (Figure 1a) or formed by more than one missing atom (Figure 1b). Structural defects are commonly generated during the CNT synthesis or by post-synthesis treatments such as electron/ion irradiation or chemical methods.[11–16] Vacancies can induce a bandgap in a metallic SWCNT, which increases the electrical resistance and renders the SWCNT semiconductive.[17,18] This feature depends on the number of vacancies and the relative position between vacancies.[17,19] In contrast, other studies have shown that in zigzag CNTs, a single vacancy can change the CNT electrical properties from semiconducting to metallic.[18,20] Modeling structural defects of CNTs by breaking individual C—C bonds has been proposed in a few works.[21,22] Structural defects such as vacancies are able to reconstruct their topology in order to minimize the formation energy.[23,24] Vacancies reduce the number of bonds by two or three bonds, with a corresponding energy reconfiguration.[25,26] Modeling the dynamic reconstruction process after bond elimination is a complex task which demands dedicated ab initio computations[27,28] which are very limited in the size of the molecule. For realistic CNT length and for polymer composites, ab initio

[*] *Dr. A. Tapia*
Facultad de Ingeniería, Universidad Autónoma de Yucatán, Av. Industrias no Contaminantes por Periférico Norte, CP 97310, Cordemex, Mérida, Yucatán, Mexico
Dr. F. Avilés, Dr. G. Domínguez-Rodríguez
Centro de Investigación Científica de Yucatán, Calle 43 No. 130, Colonia Chuburná de Hidalgo, CP97200, Mérida, Yucatán, Mexico
E-mail: faviles@cicy.mx
Dr. G. D. Seidel
Department of Aerospace and Ocean Engineering, Virginia Polytechnic Institute and State University, 228 Randolph Hall (0203) Blacksburg, VA 24061

[**] *This work was supported by CONACYT project No. 220513 of Dr. Avilés. The bilateral collaboration between CICY and Virginia Tech was possible through the CONACYT-NSF award No. 121257 (CONACYT) and OISE-1019395 (NSF). GDR acknowledges CONACYT for his PhD scholarship and the additional financial support for his visiting position at Virginia Tech. GDR also acknowledges Adarsh Chaurasia for extensive discussions and insightful ideas.*

FULL PAPER

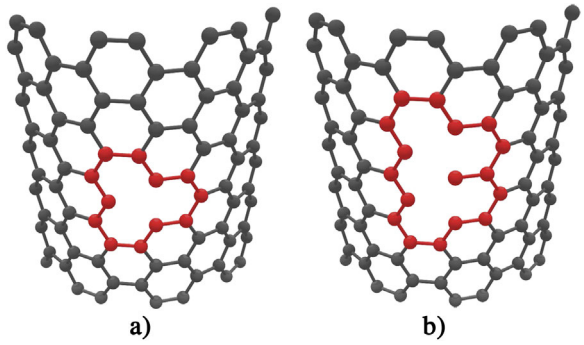

Fig. 1. Examples of topological defects present in CNTs. (a) Single vacancy, (b) double vacancy.

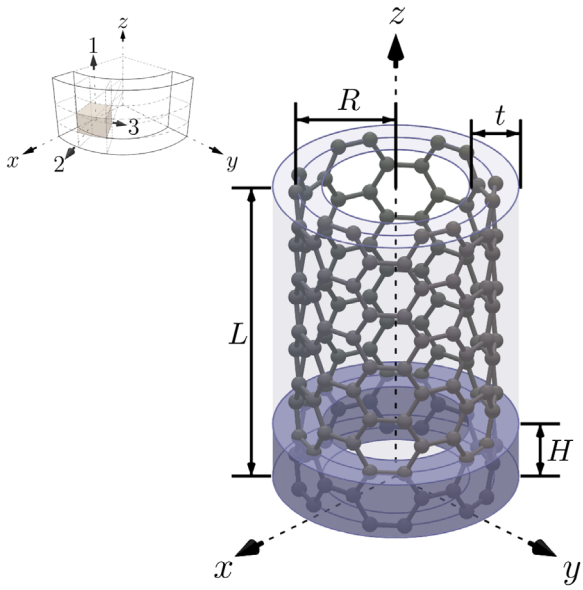

Fig. 2. Material coordinate system and geometric parameters of a typical armchair SWCNT, showing a unit cell (shadowed area).

methods are not viable due to the excessive computational burden. A classical electrostatic alternative which seems plausible for large scale problems consists of simply eliminating a bond or an atom, and using multiscale hierarchical strategies to bridge scales from that of the individual CNT to the full macroscopic nanocomposite.[29] This classical electrostatic approach is followed here by considering the nanotube as a network of metallic resistors and using the Ohm's and Kirchhoff's laws of electrostatics under appropriate boundary conditions. The structural defects are then randomly generated using two patterns (randomly dispersed or clustered) by sequentially removing C–C bonds allowing for a classical electrostatic prediction of the effects of defects on armchair (metallic) SWCNTs. In order to carry this information forward to CNT/polymer composites, the composite cylinder[30,31] and Mori–Tanaka[32] methods are employed to predict the electrical properties of axially oriented CNT/polymer bundles and composites, respectively.

2. Methodology

2.1. Electrical Properties of a Transversely Isotropic SWCNT

CNTs are treated here as transversely isotropic electrical materials which means that only two independent electrical properties are needed to construct their electrical conductivity tensor (σ_{ij}^{CNT}). Those properties are the axial electrical conductivity (σ_{11}^{CNT}) and the radial/hoop electrical conductivity (σ_{22}^{CNT}). Herein, the 1, 2, and 3 subscripts represent the axial, radial, and hoop directions of the local material coordinates of the SWCNT, respectively, whereas, x, y, and z are the orthogonal axes of the global Cartesian coordinates, see inset in Figure 2. The CNT electrical conductivity tensor is defined by,[33]

$$\sigma_{ij}^{CNT} = \begin{pmatrix} \sigma_{11}^{CNT} & 0 & 0 \\ 0 & \sigma_{22}^{CNT} & 0 \\ 0 & 0 & \sigma_{22}^{CNT} \end{pmatrix} \quad (1)$$

2.2. Atomistic Resistor Model of SWCNTs

Armchair SWCNTs of different chiralities were considered ranging from (3,3) (with a radius $R \approx 2$ nm) to (10,10) ($R \approx 7$ nm), and a total number of 200 unit cells (a total length of $L = 49.2$ nm). This length, albeit short, keeps the problem computationally tractable and was proven to yield mechanical properties which are independent of the CNT length in a previously analysis.[34] An equivalent wall thickness of $t = 3.4$ Å and a unit cell of height $H = 2.46$ Å were considered for homogenization purposes, see Figure 2.

In order to simulate the electrical conductivity of SWCNTs, an atomistic resistor model was proposed and initially validated through the evaluation of configurations with known solutions (series, parallel, and combinations of both). The C–C covalent bonds were modeled as a set of resistors following the Ohm's law; the C–C bonds of armchair CNTs are considered to be metallic, regardless of the adjacent bonds or defects, that is,

$$I_{ij} = \frac{\Phi_i - \Phi_j}{Z_{ij}} \quad (2)$$

where Z_{ij} is the electrical resistance of a C–C bond bound by atoms (nodes) i and j, I_{ij} is the current flowing between the carbon atoms i and j, and Φ_i and Φ_j are the voltages at the atoms (nodes) i and j. The Kirchhoff's circuit law is then used at each atom/node such that the current flowing into the node is balanced by the current leaving the node, that is,

$$\sum_{j=1}^{n_i} I_{ij} = 0 \quad (3)$$

where n_i is the coordination number for node i. Combining Equations 2 and 3 under the assumption that all bonds have the same resistance (Z_{bond}) yields,

$$n_i\Phi_i - \sum_{j=1}^{n_i}\Phi_j = 0 \tag{4}$$

The boundary conditions used are $\Phi_i = 0$ for grounded atoms and $\Phi_i = V_{CNT}$ for atoms where voltage is supplied. A sparse linear system is constructed from Equation 4 which is solved for the voltages. The total effective current flowing through the SWCNT is obtained from Equation 2 as,

$$I_{CNT} = \frac{1}{Z_{bond}}\sum_{i=1}^{n_g}\Phi_i \tag{5}$$

where n_g is the set of neighbors to the grounded nodes. Thus, the effective electrical resistance of the CNT (Z_{CNT}) is obtained by,

$$Z_{CNT} = \frac{\Phi_{CNT}}{I_{CNT}} \tag{6}$$

Solving Equation 6 yields Z_{CNT} which is proportional to Z_{bond}.

2.2.1. Damage Generation

The approach used here to simulate structural defects was to sequentially eliminate C–C bonds. Two configurations were investigated depending on the sequence of bond elimination followed: i) randomly generated (Figure 3a), and ii) clustered (Figure 3b). Since each carbon atom has three bonds, breakage of three bonds may be considered as a vacancy in terms of missing bonds. In the random evolution scenario, the bonds are removed by generating random numbers following a uniform distribution of probability from 0 to 1. The bond is deemed broken if the randomly generated number is lower than the fraction of broken bonds to be simulated (broken bonds/total number of bonds). Due to the random nature of the process, the computations were repeated numerous times and the results averaged, reporting the average value of the computed electrical property. A dedicated convergence analysis showed that 40 repetitions yielded differences lesser than 0.2% for all electrical conductivities and damage scenarios with respect to results with 80 repetitions, and 40 iterations were thus deemed convergent.

CNT damage was also modeled following a clustering pattern. In this approach, a 1% fraction of broken bonds was randomly generated and subsequent broken bonds were restricted to be chosen from the neighbors of the already broken ones, generating clustered damage, Figure 3b.

2.2.2. Voltage Configurations

The voltage configurations used to obtain the axial and hoop electrical conductivities of SWCNTs are depicted in Figure 4. Adequate boundary conditions to obtain the axial (Figure 4a) and hoop (Figure 4b) electrical conductivities were imposed by setting specific edge nodes to constant voltage or grounding ($V_i = 0$).

In order to obtain the axial electrical conductivity of the CNT (σ_{11}^{CNT}), all atoms at the top edge of the SWCNT ($z = L$) were set to a fixed voltage of $\Phi_i = \Delta\Phi_{CNT}$, whereas all atoms at the bottom edge ($z = 0$) were grounded ($V_i = 0$), see Figure 4a. The rest of the atoms were unrestricted and their voltages

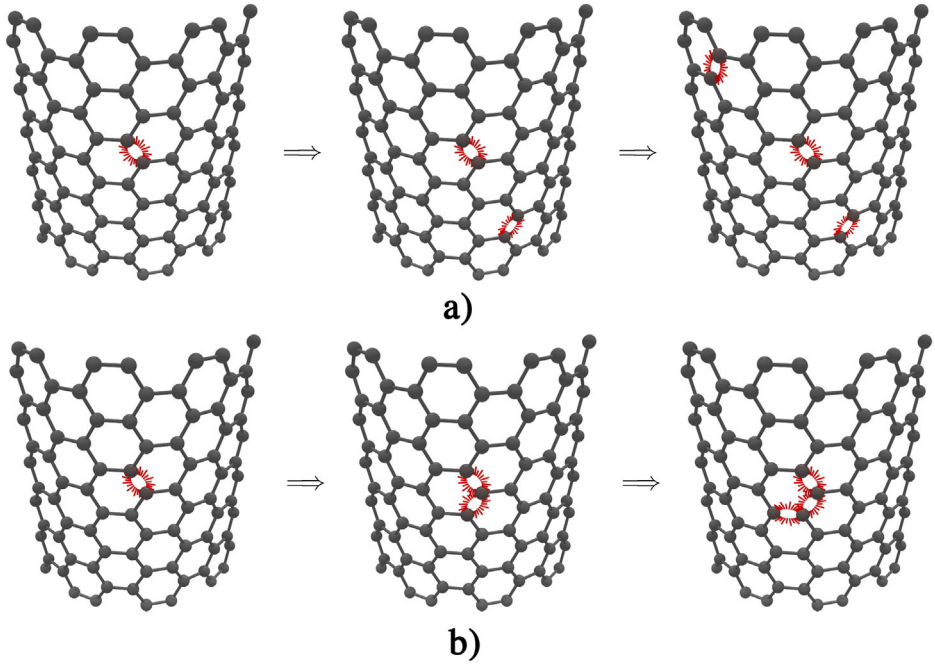

Fig. 3. Schematic representation of the two cases of damage evolution considered. (a) Random, (b) clustered.

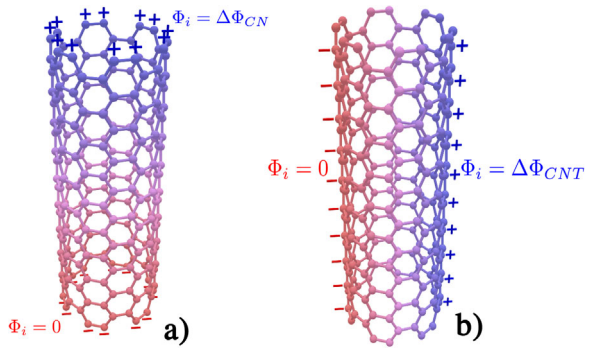

Fig. 4. Configurations used to determine the axial and hoop electrical conductivities of SWCNTs. (a) Axial electrical conductivity (σ_{11}^{CNT}), (b) hoop electrical conductivity (σ_{22}^{CNT}).

evolved to equilibrium following the Ohm's and Kirchhoff's laws. σ_{11}^{CNT} was calculated by a homogenization process, equating the resistance of the CNT given by Equation 6 to the resistance of a continuous solid cylinder (Z_{11}^{CNT}), that is,

$$Z_{11}^{CNT} = \frac{L}{\sigma_{11}^{CNT}\pi(R + t/2)^2} \tag{7}$$

Z_{bond} was obtained herein by solving Equations 6 and 7 considering a SWCNT. An axial electrical conductivity of $\sigma_{11}^{CNT} = 1 \times 10^5\,S\,m^{-1}$ was used to obtain Z_{bond} considering experimental values reported for CNTs.[35] Other values of Z_{bond} calculated for different SWCNTs are in the same order of magnitude.

For the hoop electrical conductivity (σ_{22}^{CNT}), the atoms at one side were set to a constant voltage $\Phi_i = \Delta\Phi_{CNT}$, whereas the atoms at the opposite side were grounded ($\Phi_i = 0$), see Figure 4b. σ_{22}^{CNT} was calculated by a similar homogenization process to that employed for σ_{11}^{CNT}, equating the electrical resistance of the CNT to the transverse electrical resistance of a continuous solid cylinder, which yields,[36]

$$Z_{22}^{CNT} = \frac{2}{\sigma_{22}^{CNT}\pi L}\log\left(\frac{4d}{\delta}\right) \tag{8}$$

Here, d is the chord length joining the anode and cathode ($d = 2(R + t/2)$) and δ is the assumed arc length of both the anode and the cathode. In our case, δ was considered equal to the perimeter of the SWCNT divided by the number of atoms in the unit cell ($4n_c$, where n_c is the chiral number), that is,

$$\delta = \frac{\pi(R + t/2)}{2n_c} \tag{9}$$

2.3. Prediction of Electrical Properties of Axially Oriented CNT/Polymer Composites

2.3.1. Composite Cylinder Method

The composite cylinder method (CCM) originally proposed by Hashin and Rosen[30] was used to predict the electrical properties of composite materials formed by concentric cylindrical layers. In the CCM, each layer (numbered from 1 to N) represents a phase with its own material properties, Figure 5. Here, r is the radial position and θ is the angle between the x and r axes. The CCM was employed here to predict the electrical properties of perfectly aligned polymer composites containing CNTs, including an interphase, whose elastic properties were assumed to vary linearly between those of the CNT and matrix.[41] The number of interphase layers was set to $N = 5$, which is enough to model the interphase without increasing drastically the computational burden. The center (first phase) represents the CNT, while the outermost phase (fifth phase) represents the matrix; all phases in between represent the interphase, see Figure 5. The matrix was considered an isotropic material with an electrical conductivity of $1 \times 10^{-9}\,S\,m^{-1}$ (associated with a typical epoxy polymer[37,38]). In order to model different volume fractions in the composite, the thickness of the outermost phase (matrix) was varied. The first phase (SWCNT) starts at $r = 0$ and ends at $r = R + \frac{t}{2}$, which represents the interface with the first layer of interphase. The last layer of the interphase $(N - 1)$ ends at $r = r_{N-1} = R + \frac{t}{2} + t_i$, where t_i is the interphase thickness. The thickness of the CNT/matrix interphase was set equal to the SWCNT wall thickness ($t_i = t$) as suggested by previous works.[39–41] Finally, the matrix ends at $r = r_N = R + \frac{t}{2} + t_i + t_m$, where t_m is the matrix thickness.

Since all phases have the same length (L), the volume fraction of the CNT/polymer composite (v_f) is calculated as,

$$v_f = \left[\frac{R + \frac{t}{2}}{R + \frac{t}{2} + t_i + t_m}\right]^2 \tag{10}$$

The maximum volume fraction (v_{max}) available for each CNT is obtained when $t_m = 0$.

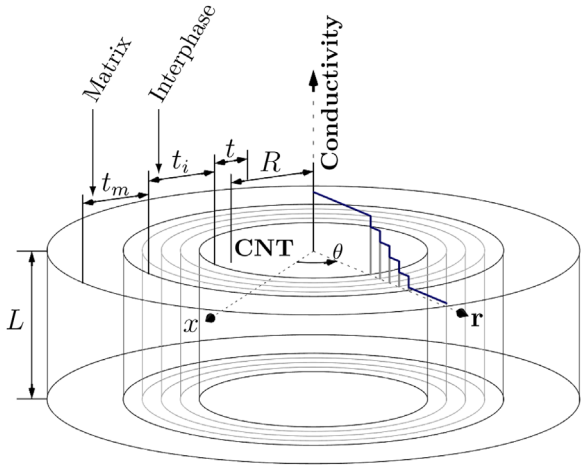

Fig. 5. Schematic of the composite cylinder model used to obtain the electrical conductivity of aligned CNT/polymer composites.

The CCM was carried out for each armchair SWCNT chirality investigated ((3,3) to (10,10)), as well as for the two scenarios of damage generation depicted in Figure 3.

2.3.2. Calculation of Axial and Transverse Composite Electrical Conductivity

Axial and transverse voltage configurations similar to those depicted in Figure 4 for SWCNTs were used to obtain the effective electrical conductivities of CNT/polymer composites (σ_{11} and σ_{22}) containing pristine and defective CNTs.

In order to calculate the axial (σ_{11}) and transverse (σ_{22}) composite electrical conductivities, axial, and transverse electrical potentials for $r_{i-1} \leq r \leq r_i$ were set as,[31,40]

$$\Phi_{ax}^{(i)} = C_1^{(i)} z + C_2^{(i)} \tag{11a}$$

$$\Phi_{tran}^{(i)} = \left(D_1^{(i)} r + D_2^{(i)} \frac{1}{r} \right) \cos\theta \tag{11b}$$

where $\Phi_{ax}^{(i)}$ and $\Phi_{tran}^{(i)}$ are, respectively, the axial and transverse electrical potential of the i-th phase and $C_1^{(i)}$, $C_2^{(i)}$, $D_1^{(i)}$, and $D_2^{(i)}$ are unknown constants.

The electric field first order tensor is defined as,

$$E_i = -\Phi_{,i} \tag{12}$$

where Φ can be either the axial (Φ_{ax}) or transverse (Φ_{tran}) electrical potential and the comma denotes spatial derivation. The electrical flux is defined as,

$$J_i = \sigma_{ij} E_j \tag{13}$$

The boundary conditions used to obtain σ_{11} specify an electrical potential along the SWCNT, that is,

$$\Phi_{ax}^{(i)}\Big|_{z=0} = 0 \tag{14a}$$

$$\Phi_{ax}^{(i)}\Big|_{z=L} = \Delta\Phi_{ax} \tag{14b}$$

where $\Delta\Phi_{ax}$ is the difference of axial electrical potential applied between $z = 0$ and $z = L$.

For the transverse electrical conductivity, the boundary condition at the outer surface of the composite ($r = r_N$) imposed on Φ_{tran} is

$$\Phi_{tran}^{(i)}\Big|_{r=r_N} = E_0 r_{N+1} \cos\theta \tag{15}$$

where E_0 is the applied electrical field. In order to avoid a mathematical singularity, $D_2^{(i)}$ in Equation 11b is set to 0 for the first layer ($i = 1$).

The continuity equations for electrical potential and electric flux are

$$\Phi_{tran}^{(i)}\Big|_{r=r_i} = \Phi_{tran}^{(i+1)}\Big|_{r=r_i} \tag{16a}$$

$$J_2^{(i)}\Big|_{r=r_i} = J_2^{(i+1)}\Big|_{r=r_i} \tag{16b}$$

Following the approach of Hashin,[30] an energy integral (W) is defined over the total volume as,

$$W = \frac{1}{2\Omega} \int_\Omega J_i E_i d\Omega \tag{17}$$

where Ω is the total volume. The energy integral for the composite cylinder assembly is set equal to the energy of an effective continuous and homogeneous cylinder, and the axial and transverse electrical conductivities for the composite cylinder assembly are obtained as,

$$\sigma_{11} = \sum_{i=1}^{N} \left(\sigma_{11}^i \frac{r_i^2 - r_{i-1}^2}{r_N^2} \right) \tag{18a}$$

$$\sigma_{22} = \frac{1}{r_N^2 E_0^2} \sum_{i=1}^{N} \sigma_{22}^i \left[\left(D_1^{(i)} \right)^2 (r_i^2 - r_{i-1}^2) - \left(D_2^{(i)} \right)^2 \left(\frac{1}{r_i^2} - \frac{1}{r_{i-1}^2} \right) \right] \tag{18b}$$

2.4. Mori–Tanaka's Approach for CNT/Polymer Composites

The Mori–Tanaka's (MT) method allows for the prediction of electrical properties of a composite material constituted by different phases, each of them with its own geometry and material properties.[32] The MT method is used here to predict the electrical conductivity tensor of a CNT/polymer composite containing randomly oriented CNTs with different chiralities and fraction of broken bonds. The electrical properties of each phase are obtained from the CCM calculations including the CNT and interphase only (matrix thickness approaches zero).

In the MT method, the electrical conductivity tensor of the composite material with axially oriented CNTs is obtained as,[32]

$$\sigma_{ij} = \sigma_{ij}^m + \sum_{l=1}^{N} v^l \left(\sigma_{ik}^l - \sigma_{ik}^m \right) A_{kj}^l \tag{19}$$

where σ_{ij}^m is the electrical conductivity tensor of the polymer matrix, σ_{ij}^l is the electrical conductivity tensor of the l-th phase (i.e., effective CNT and interphase for a specific chirality and specific fraction of broken bonds), v^l is the volume fraction of the l-th phase, and N is the total number of phases. A_{ij}^l is the non-dilute electric field concentration tensor of the l-th phase, transferring the electric field applied to the composite to the coordinate system of each embedded phase. One way to obtain A_{ij}^l is by using an Eshelby-like tensor.[42,43] Using an Eshelby-like tensor and an energetic equivalence between an inclusion with residual electric fields and the phase to be modeled, the non-dilute electric field concentration tensor for the l-th phase is,[29]

$$A_{ij}^l = \hat{T}_{ik}^l \left(M_{kj} + \sum_{o=1}^{N} v^o \hat{T}_{kj}^o \right)^{-1} \tag{20}$$

FULL PAPER

where M_{ij} is the 3×3 identity matrix, S^o_{ij} is the Eshelby-like tensor for the o-th phase, assumed as a cylindrical inclusion, and $\hat{T}^o_{ij}$ is the dilute electric field concentration tensor defined as,

$$\hat{T}^o_{ij} = \left[M_{ij} + S^o_{ik}\left(\sigma^o_{kl}\right)^{-1}\left(\sigma^o_{lj} - \sigma^m_{lj}\right)\right]^{-1} \quad (21)$$

In order to specify the total CNT volume fraction including the whole variety of CNTs used in the Mori–Tanaka formulation (V_f), initial volume fractions for each SWCNT varying the chirality and fraction of broken bonds are randomly generated following a uniform distribution of probability. A vector is formed by the randomly generated volume fractions ($\vec{v}_{\text{ini}}$). The vector of the individual volume fractions of the phases ($\vec{v}$) to be used in the MT method is defined as,

$$\vec{v} = \frac{V_f \vec{v}_{\text{ini}}}{\vec{v}_{\text{ini}} \cdot \vec{v}_{\max}} \quad (22)$$

where $\vec{v}_{\max}$ is the vector containing the maximum volume fractions of each SWCNT (when the thickness of the matrix approaches zero).

In order to compute the electrical conductivity tensor of composites containing randomly oriented SWCNTs, a rotational transformation is applied to both the dilute electrical field concentration tensor and the electrical conductivity matrix of each phase. Then, a volumetric average is applied to Equation 19 to obtain,

$$\sigma_{ij} = \sigma^m_{ij} + \sum_{o=1}^{N} \frac{v^i}{4\pi} \int_0^{2\pi} \int_0^{\pi} \left(Q_{im}\sigma^o_{ml}Q_{kl} - \sigma^m_{ik}\right) A^o_{kj} \sin\phi d\phi d\theta \quad (23)$$

where Q_{ij} is the rotational transformation matrix. The volumetric average is applied to Equation 20 to obtain the diluted electric field concentration tensor, which is given by,

$$A^o_{ij} = Q_{ik}\hat{T}^o_{kl}Q_{ml}\left(M_{mj} + \sum_{p=1}^{N} \frac{v^o}{4\pi} \int_0^{2\pi} \int_0^{\pi} Q_{mn}\hat{T}^p_{no}Q_{jo} \sin\phi d\phi d\theta\right)^{-1} \quad (24)$$

3. Results

3.1. Transversely Isotropic Electrical Properties of Defective CNTs

The electrical properties of the investigated SWCNTs were computed for the eight studied chiralities, varying from 0 to 8% fraction of broken bonds. This range is based on a fragmentation analysis as a function of the fraction of broken bonds, which suggested that after 8% fraction of broken bonds the probability of CNT fragmentation is higher than 0.9, and thus not statistically suitable for simulation. Figure 6 shows normalized plots of the axial electrical conductivity of the studied SWCNTs with both random (Figure 6a) and clustered (Figure 6b) damage. σ^{CNT}_{11} represents the axial electrical conductivity of the CNT, while $\sigma^{\text{CNT}^0}_{11}$ represents that of the pristine (defect-free) one. The axial electrical conductivity of all investigated armchair (metallic) SWCNTs decreases as the fraction of broken bonds increases. For randomly generated defects (Figure 6a), the reduction in axial electrical conductivity is similar for all chiralities with a slope of approximately 3.1. For 8% broken bonds the electrical conductivity is reduced by approximately 25%. SWCNTs with smaller radii are slightly more affected by structural defects because their unit cells have less C–C bonds (18 bonds for a (3,3) CNT) than SWCNTs with larger radii (60 bonds for a (10,10) CNT); therefore, breakage of one bond contributes more significantly to the structural integrity of smaller radius SWCNTs. The knockdown on the axial electrical conductivity as a function of the fraction of broken bonds for clustered damage (Figure 6b) presents slightly more variation among different chiralities, but similar reductions.

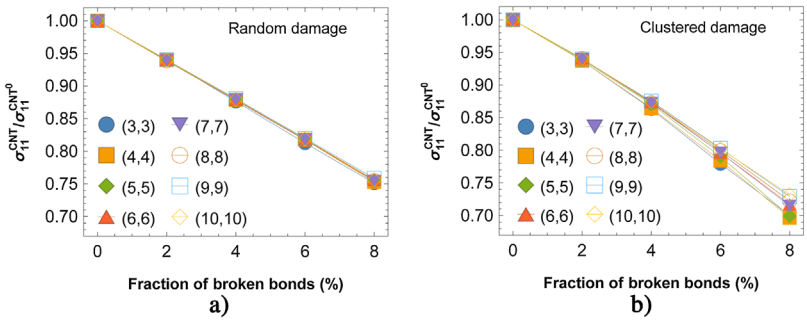

Fig. 6. Normalized axial electrical conductivity of defective CNTs as a function of fraction of broken bonds. (a) Random damage, (b) clustered damage.

The hoop electrical conductivity of SWCNTs (σ^{CNT}_{22}) was also calculated for different chiralities and fractions of broken bonds. σ^{CNT}_{22} also presents a decreasing trend with increased fraction of broken bonds (Figure 7, where σ^0_{22} is the transverse electrical conductivity of pristine SWCNTs) for all chiralities with a slope of approximately 1.8–2.5. For an 8% fraction of broken bonds, this decrement is approximately 20% with respect to the value of pristine CNTs. This behavior is more prominent for defective SWCNTs of larger radius whose unit cells have more C–C bonds. Therefore, the probability that a missing bond impedes the current flow in the transverse direction is higher if the bonds are randomly removed (Figure 7a). The situation between random and cluster is opposite for σ^{CNT}_{11} (Figure 6), since not all bonds contribute to σ^{CNT}_{11} and there are two hoop electrical conductive paths from cathode to anode for σ^{CNT}_{22}. Notice that the CNT damage influences more σ^{CNT}_{11} (Figure 6) than σ^{CNT}_{22} (Figure 7).

3.2. Axially Oriented CNT/Polymer Composites with Defective CNTs

The electrical properties of CNT/polymer composites containing axially oriented CNTs were first obtained by the

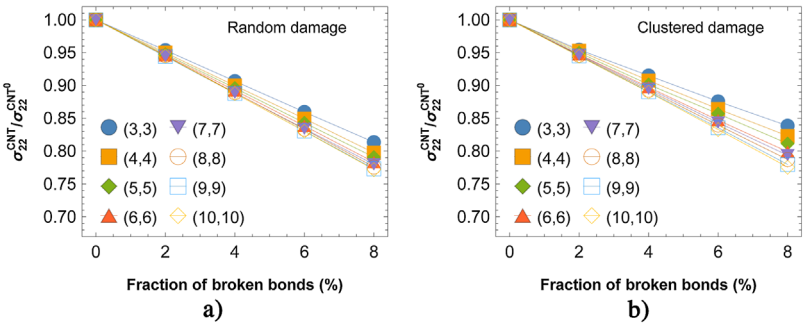

Fig. 7. Normalized hoop electrical conductivity of defective CNTs as a function of fraction of broken bonds. (a) Random damage, (b) clustered damage.

CCM for each damaged SWCNT investigated. The computations were also conducted using the Mori–Tanaka (MT) method to simulate a CNT/polymer composite containing different axially oriented SWCNTs, including the eight studied chiralities and a random distribution of fractions of broken bonds. The normalized axial electrical conductivity (axial electrical conductivity of the composite divided by the axial electrical conductivity of the polymer matrix) as a function of the SWCNT volume fraction is plotted in Figure 8a for axially oriented CNT/polymer composites. Pristine and SWCNTs containing 8% randomly generated defects are considered in Figure 8a for the thinnest (3,3) and thickest (10,10) SWCNTs investigated. The normalized axial electrical conductivity linearly increases as the volume fraction of SWCNTs increases. The axial electrical conductivity of the composite material for a volume fraction of 15% of (3,3) pristine CNTs is approximately 5×10^{13} times the axial electrical conductivity of the polymer. The axial electrical conductivity is lower for polymer composites with damaged CNTs than for those with pristine ones. As shown in Figure 8a, the normalized axial electrical conductivity of composite materials with pristine CNTs presents a higher slope (approximately 2.2×10^{14}) than that for composites containing CNTs with a fraction of broken bonds of 8% (approximately 1.6×10^{14}). Both random and clustered damages produce a very similar impact on the axial electrical conductivity as a function of the volume fraction, and thus the clustered distribution is not shown.

The transverse electrical conductivity of CNT/polymer composites was also computed by the CCM and MT methods, varying the volume fraction of CNTs as shown in Figure 8b. The four CCM predictions and the MT one present an increasing non-linear trend in σ_{22} as a function of the SWCNT volume fraction. The CCM predictions for polymer composites containing damaged and pristine SWCNTs present very similar values of the transverse electrical conductivity as a function of the volume fraction. The composites containing (10,10) SWCNTs present a lower transverse electrical conductivity than those containing (3,3) ones, following a similar trend than that found in the computations of SWCNTs (see Figure 7b).

The axial and transverse electrical conductivities of SWCNT/polymer composites as function of the SWCNT fraction of broken bonds were carried out with a fixed total volume fraction (V_f) of 1% for both random and clustered damage processes. The axial electrical conductivity of the composite (σ_{11}) normalized by the axial electrical conductivity the composite containing pristine SWCNTs (σ_{11}^0) is plotted in Figure 9 as a function of the fraction of broken bonds. σ_{11} reduces linearly with increased fraction of broken bonds, regardless of the CNT size/chirality. The composite containing (3, 3) SWCNTs shows a slightly more pronounced influence on the SWCNT fraction of broken bonds, meaning that the composites with CNTs of smaller radii are more influenced by defects. For a 8% fraction of SWCNT defects, the composite presents a knockdown in σ_{11} of approximately 25% for random damage. The polymer composites containing clustered damaged SWCNTs presented similar behavior as those with random damage but the effect of the SWCNT radius on the knockdown on the axial electrical conductivity is more pronounced.

The transverse electrical conductivity (σ_{22}) of the composite as a function of the fraction of broken bonds was also computed for composites with axially oriented CNTs, but the influence of the fraction of broken bonds was minor, and it is thus not shown. For axially oriented SWCNTs, the transverse electrical conductivity is an electrical property dominated by the polymer matrix, and hence the effect of CNT defects in such a property is minor; therefore, σ_{22} as a function of the fraction of broken bonds is not plotted.

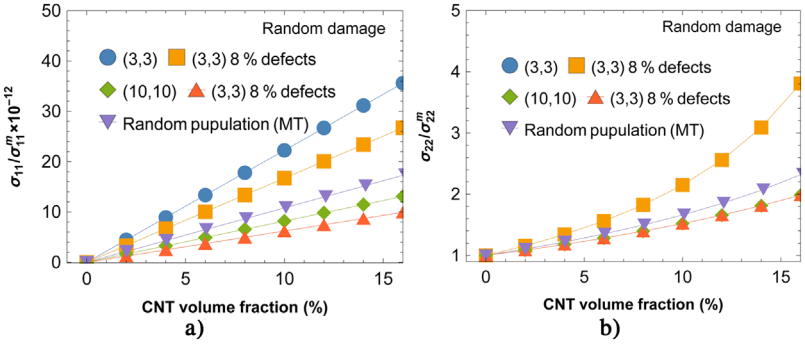

Fig. 8. Normalized electrical conductivity of CNT/polymer composites as a function of volume fraction for composites containing axially oriented CNTs. (a) Axial electrical conductivity, (b) transverse electrical conductivity.

3.3. Randomly Oriented CNT/Polymer Composites with Defective CNTs

The computations of electrical conductivity of CNT/polymer composites were also conducted for randomly oriented SWCNTs using the MT method and Equation 23, considering

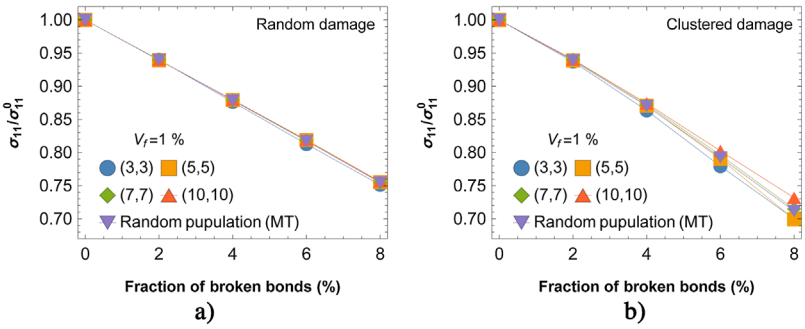

Fig. 9. Normalized axial electrical conductivity of CNT/polymer composite as a function of fraction of broken bonds for composites containing axially oriented CNTs. (a) Random damage, (b) clustered damage.

pristine and defective CNTs and a fixed volume fraction of 1%. The normalized axial electrical conductivity of CNT/polymer composites ($\sigma_{11}/\sigma_{11}^0$) as a function of the fraction of broken bonds is shown in Figure 10a for axially and randomly oriented CNTs. Both random and clustered damages present very similar trends because the CNT electrical conductivities at 8% fraction of broken bonds are of the same order of magnitude (see Figure 9); thus, only plots for random damage are shown. $\sigma_{11}/\sigma_{11}^0$ for both randomly or axially oriented CNTs presents a decreasing trend with increased fraction of broken bonds, with the slopes being indistinguishable. This is a consequence of the SWCNT contributing to the increment of the CNT/polymer composite electrical conductivity, mainly along the axial direction.

The transverse electrical conductivity of CNT/polymer composites (σ_{22}) normalized by the transverse electrical conductivity of the composite containing pristine SWCNTs (σ_{22}^0) as a function of the fraction of broken bonds is shown in Figure 10b for axially and randomly oriented CNTs. The influence of the fraction of broken bonds on $\sigma_{22}/\sigma_{22}^0$ is important only for randomly oriented SWCNTs, and causes no practical effect for axially oriented ones. This is a consequence of the minimal contribution of the axially oriented SWCNTs to the transverse electrical conductivity of the composite.

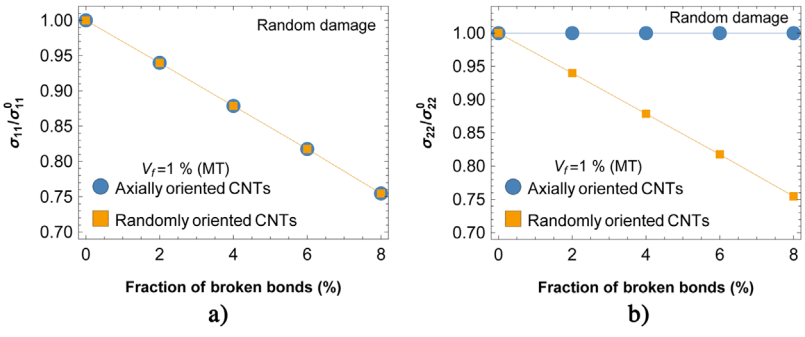

Fig. 10. Normalized electrical conductivity of CNT/polymer composites as function of the fraction of broken bonds for composites containing axially and randomly oriented CNTs. (a) Axial electrical conductivity, (b) transverse electrical conductivity.

4. Conclusions

A hierarchical multiscale approach based on a classical resistors network and micromechanics was carried out to predict the influence of CNT structural defects on the electrical properties of SWCNTs and SWCNT/polymer composites. As a first step, the electrical properties of armchair SWCNTs were modeled using a classical resistor network model. Structural defects were generated in the SWCNTs by removing carbon–carbon bonds. SWCNT damage was produced progressively by two configurations: i) randomly eliminating C–C bonds, or ii) as clustered damage by removing only the bonds that are adjacent to a small fraction of initially eliminated bonds. The axial and transverse (hoop) electrical conductivities of CNT/polymer composites were computed through the use of the composite cylinder and the Mori–Tanaka's methods. The composite cylinder method was used to model the electrical properties of a composite material containing axially oriented CNTs surrounded by an interphase. The Mori–Tanaka method was used to model composite materials containing randomly oriented CNTs with different chiralities and fraction of broken bonds. The simulations predict that 8% SWCNT structural defects yield a knockdown of 25–30% on the axial and transverse electrical conductivities of SWCNTs for both damage processes. The knockdown in axial electrical conductivity was slightly higher for cluster damage than for random damage, whereas the opposite trend occurred for the transverse electrical conductivity. The axial electrical conductivity of small radius CNTs was more affected by structural defects than that of larger radius ones, and this behavior was opposite for the transverse electrical conductivity. A similar knockdown factor to that found for defective CNTs was found for defective SWCNT/polymer composites. Modeling indicates that the composite axial electrical conductivity is the electrical property most influenced by the volume fraction of SWCNTs, and as such, this property is more influenced by the density of CNT defects at practically any concentration of SWCNTs in the composite. The transverse electrical conductivity of the CNT/polymer composites is influenced by the presence of structural defects in a similar fashion than the axial one, if the SWCNTs are randomly oriented; when the SWCNTs are axially oriented, no influence of structural defects is observed.

Quantification of the influence of defects on the electrical properties of CNTs and their polymer composites is of great importance for a more realistic assessment of the promises and limitations of these novel materials, in applications such as electronics, automotive, and aeronautics. The hierarchical multiscale approach presented here allows bridging dimensional scales, starting from

the influence of defects on an individual nanotube, and reaching effective properties of nanocomposites, of practical use for engineering estimations.

Article first published online: August 9, 2016
Manuscript Revised: July 23, 2016
Manuscript Received: March 2, 2016

[1] M. F. L. De Volder, S. H. Tawfick, R. H. Baughman, A. J. Hart, *Science* **2003**, *339*, 535.
[2] T. S. Gates, G. M. Odegard, S. J. V. Frankland, T. C. Clancy, *Compos. Sci. Technol.* **2005**, *65*, 2416.
[3] T. Fukushima, A. Kosaka, Y. Yamamoto, Y. Aimiya, S. Notazawa, T. Takigawa, T. Inabe, T. Aida, *Small* **2006**, *2*, 554.
[4] Z. Spitalsky, D. Tasis, K. Papagelis, C. Galiotis, *Prog. Polym. Sci.* **2010**, *35*, 357.
[5] M. S. Dresselhaus, G. Dresselhaus, P. H. Avouris, *Carbon Nanoubes, Topics in Applied Physics*, Vol. *80*, Springer-Verlag, Berlin/Heidelberg, Germany **2001**.
[6] S. Agrawal, M. S. Raghuveer, H. Li, G. Ramanath, *Appl. Phys. Lett.* **2007**, *90*, 193104.
[7] C. Gómez-Navarro, P. J. De Pablo, J. Gómez-Herrero, B. Biel, F. J. Garcia-Vidal, A. Rubio, F. Flores, *Nat. Mater.* **2005**, *4*, 534.
[8] L. Gao, E. T. Thostenson, Z. Zhang, T. W. Chou, *Carbon* **2009**, *47*, 1381.
[9] G. Yin, N. Hu, Y. Karube, Y. Liu, Y. Li, H. Fukunaga, *J. Compos. Mater.* **2011**, *45*, 1315.
[10] P. T. Araujo, M. Terrones, M. S. Dresselhaus, *Mater. Today* **2012**, *15*, 98.
[11] F. Banhart, J. Kotakoski, A. V. Krasheninnikov, *ACS Nano* **2010**, *5*, 25.
[12] R. Balog, B. Jø rgensen, L. Nilsson, M. Andersen, E. Rienks, M. Bianchi, M. Fanetti, E. Lægsgaard, A. Baraldi, L. Lizzit, *Nat. Mater.* **2010**, *9*, 315.
[13] F. Banhart, *Rep. Prog. Phys.* **1999**, *62*, 1181.
[14] K. S. Kim, Y. Zhao, H. Jang, S. Y. Lee, J. M. Kim, K. S. Kim, J. H. Ahn, P. Kim, J. Y. Choi, B. H. Hong, *Nature* **2009**, *457*, 706.
[15] A. Krasheninnikov, F. Banhart, *Nat. Mater.* **2007**, *6*, 723.
[16] M. M. Lucchese, F. Stavale, E. H. Martins Ferreira, C. Vilani, M. V. O. Moutinho, R. B. Capaz, C. A. Achete, A. Jorio, *Carbon* **2010**, *48*, 1592.
[17] Y. Fan, B. R. Goldsmith, P. G. Collins, *Nat. Mater.* **2005**, *4*, 906.
[18] W. Orellana, P. Fuentealba, *Surf. Sci.* **2006**, *600*, 4305.
[19] H. Y. Qian, T. Zhou, *Sci. China Phys. Mech. Astron.* **2010**, *53*, 11.
[20] E. Faizabadi, in *Electronic Properties of Carbon Nanotubes* (Ed: J. M. Marulanda), InTech, Rijeka, Croatia **2011**, p. 603.
[21] M. Ouyang, J. L. Huang, C. L. Cheung, *Science* **2001**, *292*, 702.
[22] A. Zandiatashbar, G. H. Lee, S. J. An, S. Lee, N. Mathew, M. Terrones, *Nat. Commun.* **2014**, *5*, 1.
[23] S. Berber, A. Oshiyama, *Phys. B* **2006**, *376–377*, 272.
[24] J. Yuan, K. M. Liew, *Carbon* **2011**, *47*, 1526.
[25] S. L. Mielke, D. Troya, S. Zhang, J. L. Li, S. Xiao, R. Car, R. S. Ruoff, G. C. Schatz, T. Belytschko, *Chem. Phys. Lett.* **2004**, *390*, 413.
[26] K. I. Tserpes, P. Papanikos, *Compos. Struct.* **2007**, *79*, 581.
[27] W. Koch, M. C. Holthausen, *A Chemist's Guide to Density Functional Theory*, 2nd Ed., Wiley-VCH, Weinheim, Germany **2001**.
[28] D. C. Young, *Computational Chemistry*, John Wiley & Sons, Inc., New York, USA **2001**.
[29] G. D. Seidel, D. C. Lagoudas, *J. Compos. Mater.* **2009**, *43*, 917.
[30] Z. Hashin, B. Rosen, *J. Appl. Mech.* **1964**, *31*, 223.
[31] Z. Hashin, *Mech. Mater.* **1990**, *8*, 293.
[32] T. Mori, K. Tanaka, *Acta Metall.* **1973**, *21*, 571.
[33] J. M. Qu, M. Cherkaoui, *Fundamentals of Micromechanics of Solids*, John Wiley & Sons, Inc., Hoboken, New Jersey, USA **2006**.
[34] G. Domínguez-Rodríguez, A. Tapia, F. Avilés, *Comput. Mater. Sci.* **2014**, *8*, 257.
[35] T. Ebbesen, H. Lezec, H. Hiura, J. Bennett, H. Ghaemi, T. Thio, *Nature* **1996**, *382*, 54.
[36] J. Jeans, *The Mathematical Theory of Electricity and Magnetism*, 5th Ed., Cambridge University Press, Cambridge, UK **1911**.
[37] J. K. W. Sandler, J. E. Kirk, I. A. Kinloch, M. S. P. Shaffer, A. H. Windle, *Polymer* **2003**, *44*, 5893.
[38] Q. Wang, J. Dai, W. Li, Z. Wei, J. Jiang, *Compos. Sci. Technol.* **2008**, *68*, 1644.
[39] G. D. Seidel, D. C. Lagoudas, S. J. V. Frankland, T. S. Gates, "Modeling functionally graded interphase regions in carbon nanotubes reinforced composites," *20th Annual Technical Conference*, American Society for Composites, Philadelphia, USA **2005**, 7.
[40] G. D. Seidel, Micromechanical Modeling of the Multifunctional Nature of Carbon Nanotube-Polymer Nanocomposites. PhD Dissertation, Texas A&M University **2007**.
[41] A. Hernández-Pérez, F. Avilés, *Comput. Mater. Sci.* **2010**, *47*, 926.
[42] J. Eshelby, *Proc. R. Soc. London* **1957**, *241*, 376.
[43] J. Eshelby, *Proc. R. Soc. London* **1959**, *252*, 561.

